Soft Matter

View Online
Dynamic Article Links

Cite this: DOI: 10.1039/c1sm05944k

www.rsc.org/softmatter

PAPER

Dynamics of the contact line in wetting and diffusing processes of water droplets on hydrogel (PAMPS–PAAM) substrates

Tadashi Kajiya,[a] Adrian Daerr,[a] Tetsuharu Narita,[b] Laurent Royon,[a] François Lequeux[b] and Laurent Limat[a]

Received 20th May 2011, Accepted 18th August 2011
DOI: 10.1039/c1sm05944k

We studied the dynamics of the wetting and diffusing processes of water droplets on hydrogel (Poly(2-acrylamido-2-methyl-propane-sulfonic acid -*co*- acrylamide) (PAMPS–PAAM)) substrates. The profiles of the droplet and substrate were measured simultaneously using a grid projection method. We observed that as the water droplet diffuses into the gel, the contact line of the droplet exhibits successively two different behaviors: pinned and receding, and the transition between these two behaviors is closely related to the local deformation of the gel substrate. The contact line is pinned at an early stage. As the water diffusion proceeds, the contact angle of the droplet decreases while the angle of the local slope of the gel surface near the contact line increases. At the moment where these two angles almost correspond to each other, the contact line starts to recede. Our results indicate that due to the water diffusion, a locally swollen region is formed in the vicinity of the droplet–gel interface, and whether the contact line is pinned or recedes is determined by the surface property of this swollen region.

I. Introduction

Gels are materials which have been attracting continued interest as they are an intriguing state of matter in physical and chemical sciences[1] and they also have promising technological potentials in many application fields such as food processing, drug delivery,[2] and cell transplantation.[3] The understanding and control of interfacial properties of gels is of crucial importance in applications: they determine adhesion and friction[4,5] (*e.g.* cartilage replacement), surface tension[6] and wetting properties (*e.g.* soft coatings), optical properties[7] (*e.g.* anticondensation coatings), effects on bacterial motility,[8] *etc.* Of those problems about the interfacial properties of gels, here we are focusing on the problem of wetting.

Compared to general solid materials on which wetting problems have been extensively studied,[9–11] gels have two specific features which can affect the behavior of the contact line, *i.e.*, gels are very soft and swell drastically with liquid. Considering these two aspects, the behavior of the contact line of liquid on gel surfaces might be understood in analogy with the wetting problems on soft and deformable surfaces like elastomers,[12–17] or the wetting problems on permeable surfaces like porous media or polymer films.[18,19] Although the effect of the softness and the liquid permeability were studied separately, the behavior of the contact line on gel surfaces would be yet different from those cases because these two aspects exist simultaneously. Several studies have been conducted to characterize the wetting properties on gel surfaces,[20–22] but these studies did not make clear how the behavior of the contact line is different when it is coupled with the local deformation of the substrate and the diffusion of the liquid.

In this article, we studied the wetting and diffusing processes of water droplets on hydrogel (Poly(2-acrylamido-2-methyl-propane-sulfonic acid -*co*- acrylamide)(PAMPS–PAAM)) substrates. The precise analysis of the contact line behavior in the presence of the substrate deformation and liquid diffusion requires measurement of both the profiles of the droplet and of gel substrate simultaneously. In a static case, the simultaneous measurement of the profiles of the droplet and of the substrate was conducted by fluorescent microscopy for liquid droplets on elastomer surfaces.[23–25] To obtain these two profiles dynamically, we used the "grid projection method", *i.e.*, we projected a grid pattern below the gel surface and measured its optical distortion induced by the light refraction at the surface to reconstruct the original profile.

The use of a grid pattern for measuring the profile of a liquid surface has been proposed by Kurata *et al.*[26] and Fermigier *et al.*[27] in the problems of free surface flows, and by Andrieu *et al.*[28] in the dewetting problem of thin liquid films. Recently, Banaha *et al.* reported that the same technique can be applied to measure the spreading process of liquid on Agar gels,[29] in which they measured both the surface profiles of the liquid and of the gel. Here we have improved the method of Banaha *et al.* by extending the optical setup so that a reduced mirror image of the grid pattern is projected inside the gel and is used for the profile

[a]*Laboratoire MSC, UMR 7057, CNRS, Université Paris Diderot, Bâtiment Condorcet, 10 rue Alice Domon et Léonie Duquet, 75205 Paris Cedex 13, France*
[b]*PPMD-SIMM, UMR 7615, CNRS, UPMC, ESPCIParisTech, 10 rue Vauquelin, 75231 Paris Cedex 05, France*

measurement. This allows for a considerably higher spatial resolution.

We observed that as the water droplet diffuses into the gel substrate, the behavior of the contact line exhibits successively two different regimes: pinned and receding, and the transition between these two regimes is closely related to the local deformation of the substrate around the contact line. We discuss how the pinned–receding transition depends on the properties of the gel, *i.e.*, the rigidity and hydrophilicity (tuned by the concentrations of crosslinking agent and of hydrophilic AMPS monomer), which determine the gel swelling ability. In chapter IV, we propose possible mechanisms for the behavior of the contact line.

II. Experimental section

A. Materials

Poly(2-acrylamido-2-methyl-propane-sulfonic acid *-co-* acrylamide) (PAMPS–PAAM) gels were used for gel substrates and distilled water (Milli-Q Integral; Millipore, USA) was used for liquid droplets. The PAMPS–PAAM gels were prepared through the radical polymerization of a solution of 2-acrylamido-2-methyl-propane-sulfonic acid (AMPS; Sigma-Aldrich, USA) and acrylamide (AAM; Alfa Aesar, USA) in water with a crosslinking agent, *N*,*N*′-methylenebisacrylamide (MBA; Sigma-Aldrich, USA), and initiators, Potassium persulfate (PS; Sigma-Aldrich, USA) and *N*,*N*,*N*′,*N*′-Tetramethylenediamine (TEMED; Sigma-Aldrich, USA). The total molar concentration of monomer was fixed at 1 M. The concentrations of AMPS and of crosslinking agent MBA with respect to the total amount of monomer were tuned as control parameters: C_{AMPS} was set at 10 mol% and 30 mol%, and C_{MBA} was changed from 1 mol% to 20 mol%. Note that C_{MBA} changes the rigidity of the gel, while C_{AMPS} corresponds the fraction of hydrophilic monomers and thus changes the hydrophilicity of the gel. The concentrations of initiators PS and TEMED were fixed at 1 mol%.

To obtain a sheet-shaped gel substrate with a smooth surface, the gel was prepared between two parallel glass slides which were separated by a silicone rubber spacer with a thickness of 4.5 mm, which always remains large compared to the radius (<1.5 mm) and height (<0.45 mm) of the droplet. Before being used, glass slides were pre-cleaned with a 1 M solution of sodium hydrate in ethanol for 1 week. The polymerization was started by heating a monomer solution to 60 °C in a heat chamber. For the polymerization to finish completely, the solution was kept in a heat chamber for 2 h then at room temperature for more than 3 days before it was used for the measurement. The surface roughness of the gel is not known but should not exceed that of the glass surface, *i.e.*, a few tenths of nanometres.

To check the swelling ability of the gel, the volume change of the gel was measured between at the initial state and at the fully swollen state. Here, the fully swollen gel was prepared by dipping the gel in a water bath for more than 1 week. Fig. 1 shows the plots of the volume swelling ratio, *i.e.*, the relative volume of the gel at the fully swollen state $V^{\mathrm{sw}}_{\mathrm{gel}}$ to at the initial state V^{i}_{gel}, against the MBA concentration C_{MBA} in two different AMPS concentrations C_{AMPS}. It is seen that the gel swells drastically with water, and that both the parameters C_{AMPS} and C_{MBA} affect the swelling ability of the gel. For high C_{AMPS} and low C_{MBA}, the gels are swollen up to more than 10 times their initial volumes, while for low C_{AMPS} and high C_{MBA}, the gels are swollen only to less than twice the initial volumes.

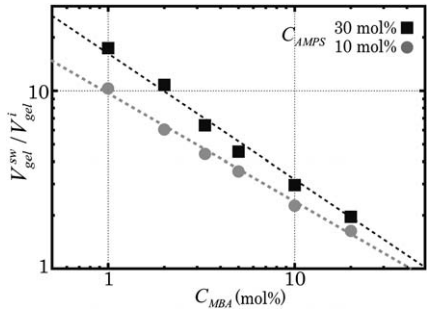

Fig. 1 A plot of the volume swelling ratio: relative volume of the gel at the fully swollen state to the initial state $V^{\mathrm{sw}}_{\mathrm{gel}}/V^{i}_{\mathrm{gel}}$, against the MBA concentration. The data of two different AMPS concentrations (10 mol% and 30 mol%) are plotted with different symbols.

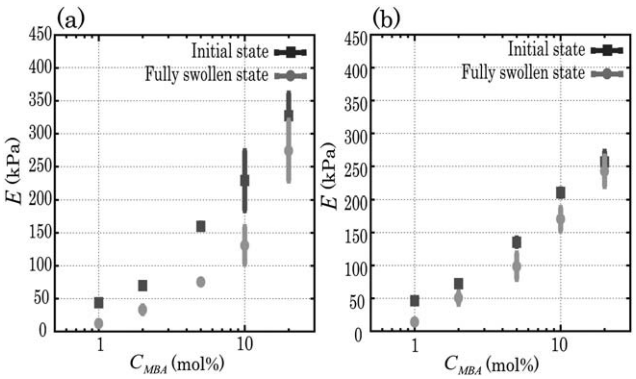

Fig. 2 A plot of the elasticity of the gel against the MBA concentration. The AMPS concentrations were 30 mol% for (a) and 10 mol% for (b). In each figure, data of gels at the initial states (before swelling) and at the fully swollen states are plotted with different symbols.

The elasticity of the gel was measured by an indentation tester (TA.XTPlus; Texture Technologies, USA) with a spherical probe ($\phi = 0.5$ inch) and was plotted in Fig. 2. The refractive index of the gels were measured with a refractometer (ARAGO®; Cordouan Technologies, France) as 1.350 ± 0.003 for the gels $C_{\mathrm{AMPS}} = 30$ mol% and 1.346 ± 0.003 for $C_{\mathrm{AMPS}} = 10$ mol%, which are considerably close to the value of water: 1.331.

B. Setup for profile measurement

Fig. 3(a) shows the setups for the profile measurement. A gel substrate was placed on a hollow stage, and a droplet was placed on the substrate with a micropipet. The initial volume of the droplet V^{i}_{drop} was fixed at 1 μl. As the gel is initially under the swelling equilibrium, the droplet of 1 μl completely diffuses into the gel. To restrain the effect of water evaporation from the droplet and from the gel, the droplet and gel substrate were sealed by a small plastic box in which air was saturated with water vapor. This has been performed by depositing a ring of water all around the gel (note that the water ring does not touch the gel).

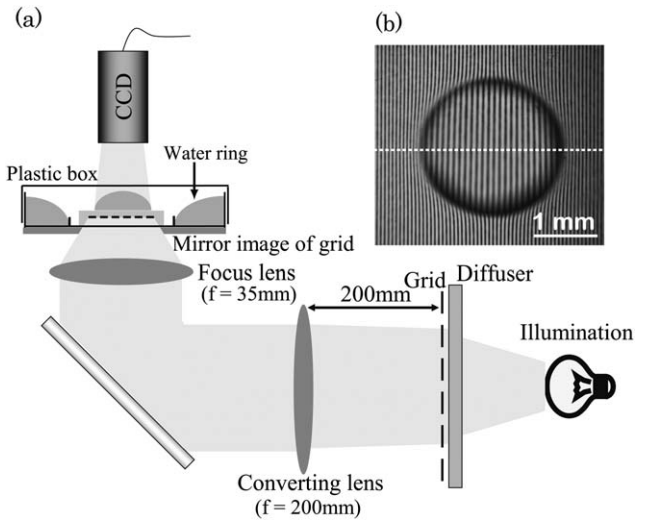

Fig. 3 (a) A schematic of the setup for the profile measurement. Using two lenses (converting lens: $f = 200$ mm, focus lens: $f = 35$ mm), the mirror image of the grid was projected inside the gel which was located just below the droplet. (b) An image of grid lines which is taken after the droplet is placed on the gel substrate. Due to the deformation of the interface (air–water and air–gel), the grid lines are distorted and their apparent spacing has changed.

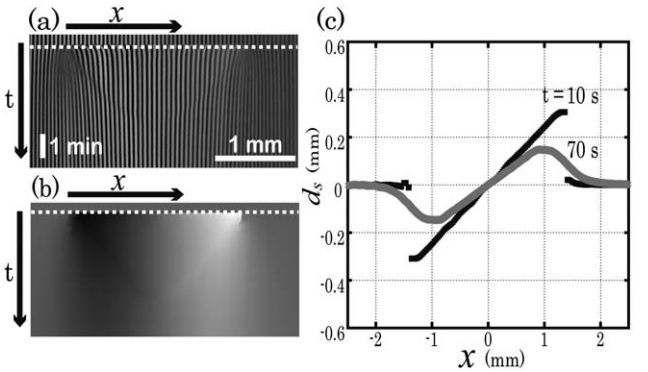

Fig. 4 (a) A spatio–temporal diagram of the grid lines in one cross section of the droplet. (b) A spatio–temporal diagram of the shift distances of lines d_s. d_s is proportional to a gray-scale: the dark region means that the grid shifts to the left and the bright region indicates the grid shifts to the right. In figures (a) and (b), the dashed line indicates the time that the droplet is placed. (c) Profiles of the shift distances d_s at two different times (10 and 70 s). The position $x = 0$ indicates the center of the droplet and the shift distance becomes positive when the line shifts to the right. For all figures, the MBA and AMPS concentrations of the substrate are 5 and 30 mol%, respectively.

To measure both the profile of the droplet and gel simultaneously, a grid projection method was used. In the grid projection method, the profile of the object is obtained by tracing a optical distortion of grid lines. The original grid plate (Array of black lines printed on a transparency. The distance of each line was 400 μm.) was located far from the observation system. The illumination light was emitted from the photodiode (Lumileds; Philips, Netherlands) and passed through the grid plate. After being converted to a parallel light by an optical lens ($f = 200$ mm), the light was guided toward the bottom of the substrate, and passed through a focus lens (TV lens $f = 35$ mm; Pentax, Japan). This focus lens projects the mirror image of the grid inside the gel substrate, whose position was set just below the droplet. In all measurements, the depth of the mirror image from the gel surface was fixed at $e_0 = 1.875$ mm. The grid image was measured with a CCD camera (A101FC; Basler AG, Germany) with a magnification lens (TV lens $f = 25$ mm; Pentax, Japan) placed above the droplet.

Fig. 3(b) shows the image of the grid lines obtained after the droplet is placed on a gel substrate. In the mirror image, the distance of each grid line was 59.5 μm, thus the resolution increases up to 6 times of the original grid lines. For analysis, one cross section of the droplet which is perpendicular to the grid lines (indicated in Fig. 3(b) as a dashed line) was used.

III. Experimental results

A. Shift of grid lines and reconstruction of profile

Fig. 4(a) shows the spatio–temporal diagram of grid lines in one cross section of the droplet. It is seen that after the droplet is placed on a substrate, the grid lines in the region of the droplet appear shifted from their initial positions by certain distances. In the left side of the droplet, the lines shift to the left, while the lines shift to the right in the right side.

Using an image analysis, the positions of all lines (center of black lines and white lines) were detected and were tracked over time, yielding the distance of shift d_s with respect to the unperturbed grid. Fig. 4(b) shows the spatio–temporal diagram of the shift distance of grid lines $d_s(x, t)$ and Fig. 4(c) shows the plot of d_s at two different times. Note that in both figures, the data of d_s between the positions of grid lines was linearly interpolated.

Just after the droplet is placed on a substrate ($t = 10$ s), a large discontinuity of d_s exists between the region where the droplet was placed and the outer region, *i.e.*, d_s varies sharply at the edge of the droplet. As the water diffuses from the droplet to the gel ($t = 70$ s), d_s becomes smaller in the droplet region, while the region that d_s has a non-zero value extends outwards from the initial position of the edge of the droplet.

As is shown in Fig. 5(a), the shift of grid lines is due to the refraction of lights at the interface between the mediums of different refractive indexes (medium A: air, medium B: water or gel). With geometrical optics, the value of the shift distance $d_s(x, t)$ is related to the local slope of the interface $\tan \alpha(x, t)$ by the following three equations:

$$\sin \alpha = n \sin \beta, \tag{1}$$

$$\delta = \alpha - \beta, \tag{2}$$

$$\tan \delta = \frac{d_s}{e}, \tag{3}$$

where α and β are the angles of the light path in mediums A and B with respect to the normal to the interface, δ is the angle of the light path in medium B with respect to the vertical axis z, n is the refractive index of medium B (since n of the PAMPS–PAAM gel is sufficiently close to the value of water, we used the value of water $n = 1.33$ for both droplet and gel regions), and $e(x, t)$ is the depth of the grid lines from the interface. At a point $x = x_0$

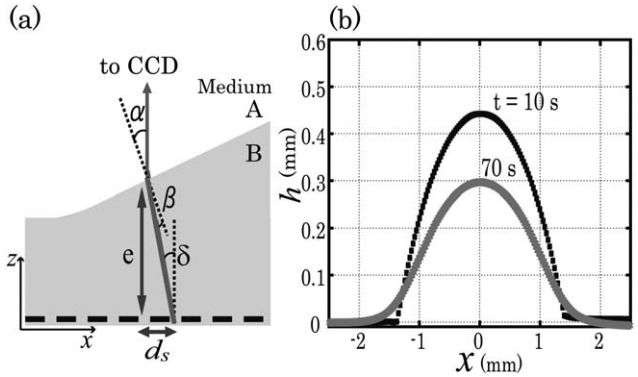

Fig. 5 Reconstruction of the profile. (a) Geometry of the light path that passes the grid image and is detected by the CCD. As the interface between two mediums A (air) and B (water or gel) of different refractive indexes is inclined with respect to the horizontal axis x, the light is refracted at the interface. (b) Reconstructed profiles of the droplet obtained from the data in Fig. 4(c). Profiles at two different times (10 and 70 s) are plotted.

located sufficiently far from the droplet, we can consider that $\alpha_0 = 0$ and that $e(x_0)$ still remains the initial value e_0 before the droplet is placed. From there, $\alpha(x)$ and $e(x)$ are calculated numerically by integrating eqns (1)–(3) and the relation

$$e(x) = e_0 + \int_{x_0}^{x} dx' \tan\alpha(x'), \tag{4}$$

at each data point. Fig. 5(b) shows the profiles $h(x) = e(x) - e_0$ of the droplet and substrate reconstructed from the data in Fig. 4 (c). Here, the calculation was conducted from left $x < 0$ to right $x > 0$.

B. Relation between behavior of contact line and deformation of substrate

Fig. 6(a) shows the half cross sections of the profiles (the height h against the radial position r) of the droplet and gel substrate at different times (Substrate: $C_{MBA} = 5$ mol% and $C_{AMPS} = 30$ mol%). During the diffusion process of the droplet into the gel substrate, both the profiles of the droplet and substrate change. At an early stage ($t = 25$ s), the contact line of the droplet is seen clearly, *i.e.*, the slope of the profile is discontinuous at the droplet perimeter. As the water diffusion proceeds, the height of the droplet decreases, while the height of the gel substrate around the contact line increases. The horizontal extent of the substrate deformation grows close to the order of 1 mm from the initial position of the contact line, and the boundary between the droplet and substrate becomes less clear.

Although the contact line is difficult to observe directly at the late stage, it is still possible to detect the position of the contact line using the local curvature of the profile at the center ($r \approx 0$). When a water droplet still resides on the gel substrate, the surface of the central region where the droplet resides must be a spherical cap of uniform curvature due to the effect of the surface tension. Therefore, if the local curvature at the center H_c is calculated as:

$$\frac{1}{H_c} \approx \left.\frac{\partial^2 h}{\partial r^2}\right|_{r\approx 0}, \tag{5}$$

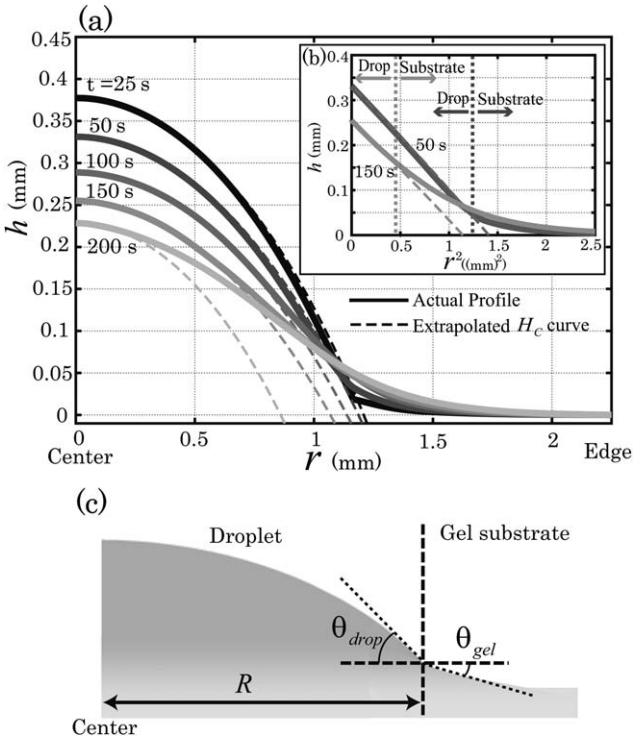

Fig. 6 (a) Half cross sections of the profiles of the droplet and substrate ($C_{MBA} = 5$ mol%, $C_{AMPS} = 30$ mol%) at 5 different times (25, 50, 100, 150 and 200 s). The solid lines indicate the actual profiles, while the dashed lines indicate the extrapolations of the local curvatures at the center H_c. (b) A replot of the height h against the second power of the radial position r^2. The positions of the contact lines where the actual profiles deviate from the extrapolated H_c curves are marked as dotted lines. (c) The definition of parameters R, θ_{drop}, and θ_{gel}.

and then it is extrapolated outward, the position of the contact line can be detected as the point where the actual profile deviates from the extrapolated H_c curve. The extrapolated H_c curves are also plotted in Fig. 6(a) as dashed lines. To show the position of the contact line more clearly, h is replotted as a function of r^2 in Fig. 6(b).

Now that the position of the contact line has been detected, it is possible to measure the radius of the droplet R, the effective contact angle of the droplet θ_{drop} with respect to horizontal, and the angle of the local slope of the gel surface θ_{gel} close to the contact line. Fig. 6(c) illustrates the determination of R, θ_{drop} and θ_{gel}. The angle θ_{drop} was calculated from the radius of the droplet R and the curvature H_c as:

$$\theta_{drop} = \sin^{-1}(R/H_c), \tag{6}$$

while θ_{gel} was directly measured from the slope of the profile in the vicinity of the contact line (The position used for measuring θ_{gel} was 1.5 grid spacings ($\approx$90 μm) apart from the position of the contact line.). Fig. 7 shows the plot of R against the time t, and Fig. 8 shows the plot of θ_{drop} and θ_{gel} against t. In both figures, data of two different substrates are shown: (a) $C_{AMPS} = 30$ mol% and $C_{MBA} = 5$ mol%, (b) $C_{AMPS} = 10$ mol% and $C_{MBA} = 5$ mol%.

In Fig. 7, although the time scales are different on these two substrates, the general trends are almost the same: the behavior

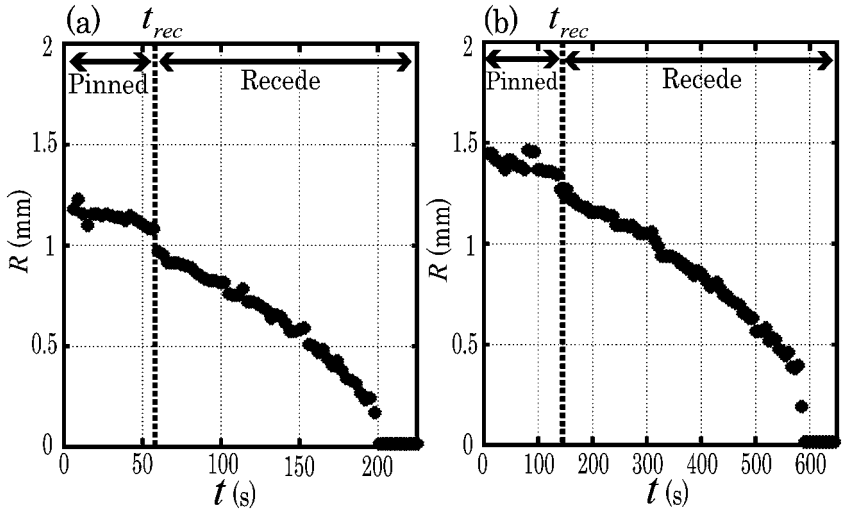

Fig. 7 Plots of the radius of the droplet (the region having a same curvature as the center) R against the time t. The MBA concentration C_{MBA} is fixed at 5 mol%, and the AMPS concentrations C_{AMPS} are (a) 30 mol% and (b) 10 mol%.

of the contact line exhibits two different regimes. The contact line is initially pinned, *i.e.*, it does not move during a certain period. At a time $t = t_{rec}$, the contact line starts to recede and then it continues to recede until the droplet has totally diffused into the gel. By comparing Fig. 7 to Fig. 8, it is clearly observed that the transition of the pinning to receding regimes of the contact line is closely related to the time evolutions of θ_{drop} and θ_{gel}. At the initial stage where the contact line is pinned, the values of θ_{drop} and θ_{gel} are largely different. As the water diffusion proceeds, these two angles come close to each other: θ_{drop} decreases while θ_{gel} increases. At the moment where θ_{drop} and θ_{gel} almost correspond, the contact line starts to recede. This result indicates that at the moment of the contact line recession, the actual contact angle of the droplet with respect to the substrate $\Delta\theta = \theta_{drop} - \theta_{gel}$ is nearly 0°. The same trend was observed for all AMPS and MBA concentrations in our experiment.

C. Dependence on properties of gel substrate

In this section, we show how the behavior of the contact line depends on the following parameters: the MBA concentration C_{MBA} that determines the rigidity of the gel substrate and the PAMPS concentration C_{AMPS} that determines the hydrophilicity of the substrate.

Fig. 9(a) shows the plot of the radii of droplets R against the time t on the substrates of two different C_{MBA} (2 and 10 mol%), where C_{AMPS} is fixed at 10 mol%. For the sake of comparison, the radius R and time t are normalized respectively by the initial radius R_i and total diffusion time t_f defined as the time at which the droplet has completely diffused into the gel. Fig. 9(a) shows that the relative length of the initial pinned regime to the total diffusion time t_{rec}/t_f depends upon C_{MBA} of the substrate. For low C_{MBA} (2 mol%) where the rigidity of the substrate is weak, the initial pinned regime is considerably short relative to the total

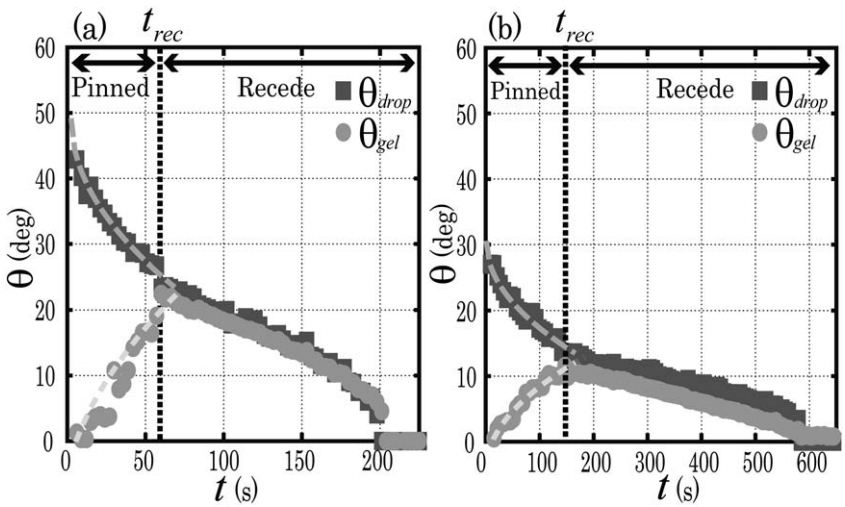

Fig. 8 Plots of the angles of the droplet θ_{drop} and gel substrate θ_{gel} with respect to horizontal against the time t. The MBA concentration C_{MBA} is fixed at 5 mol%, and the AMPS concentrations C_{AMPS} are (a) 30 mol% and (b) 10 mol%. In the left part of each figure, the fitting curves of the theoretical model proposed in section IV B are marked as gray dashed lines.

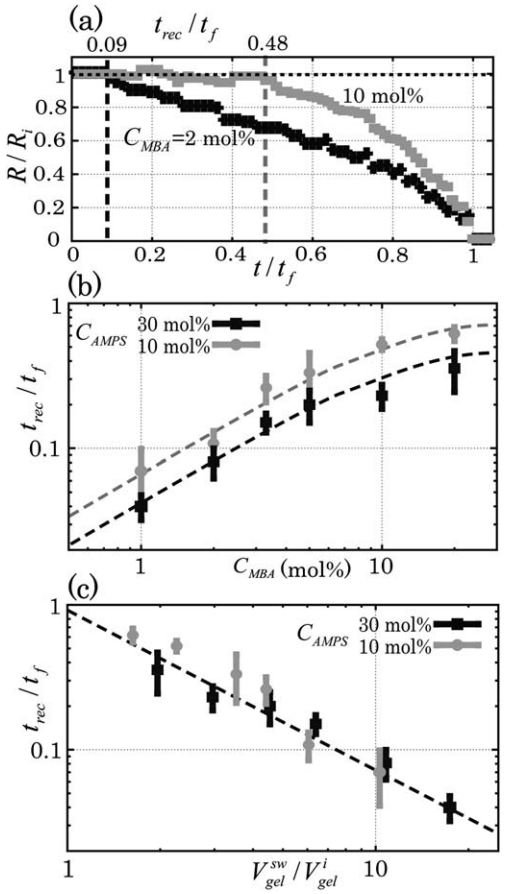

Fig. 9 (a) A plot of the normalized radius of the droplet R/R_i against the normalized time t/t_f (C_{AMPS} = 10 mol%). Data of two different MBA concentrations C_{MBA} (2 and 10 mol%) are plotted. The times when the contact line recession starts t_{rec}/t_f are marked as dashed lines. (b) A plot of t_{rec}/t_f against C_{MBA}. Data of two different C_{AMPS} (10 and 30 mol%) are plotted with different symbols. (c) A replot of t_{rec}/t_f against the volume swelling ratio V_{gel}^{sw}/V_{gel}^{i}.

diffusion time (t_{rec}/t_f = 0.09). The contact line starts to recede immediately after the droplet is placed on the substrate. On the other hand, for high C_{MBA} (10 mol%) where the substrate is more rigid, the initial pinned regime becomes relatively long, *i.e.*, the contact line is pinned almost the half period of the whole diffusion process (t_{rec}/t_f = 0.48).

To evaluate the parameter dependence in detail, the relative length of the initial pinned regime to the total diffusion time t_{rec}/t_f was measured on gels of various C_{MBA} and C_{AMPS}, and was plotted in Fig. 9(b). For both C_{AMPS}, t_{rec}/t_f becomes longer with the increase of C_{MBA}, *i.e.*, the contact line is pinned for a longer time with the increase of the gel rigidity. Comparing the data of different C_{AMPS}, it is observed in a whole range of C_{MBA} that t_{rec}/t_f is shorter for higher C_{AMPS} (30 mol%), *i.e.*, the contact line starts to recede earlier when the gel substrate has higher hydrophilicity.

In Fig. 1, it was seen that both the parameters C_{MBA} and C_{AMPS} largely affect the swelling ability of the gel, *i.e.*, the volume swelling ratio V_{gel}^{sw}/V_{gel}^{i}. Considering that, the data t_{rec}/t_f for all gels are replotted as a function of V_{gel}^{sw}/V_{gel}^{i} in Fig. 9(c). It is clearly observed that t_{rec}/t_f has a universal negative dependence upon V_{gel}^{sw}/V_{gel}^{i}.

IV. Discussion

A. Mechanism of contact line recession with a nearly zero contact angle: formation of a locally swollen region

In this section, we discuss why the actual contact angle of the droplet $\Delta\theta = \theta_{drop} - \theta_{gel}$ becomes nearly 0° at the moment of the contact line recession. Fig. 10 shows the schematics of the physical model we propose.

After the droplet is placed on a gel substrate, the water starts to diffuse from the droplet into the substrate (here we assume that the effect of the evaporation is considerably smaller than of the diffusion into the substrate), and the gel substrate deforms as it swells with water. From the fact that the horizontal size of the deformation of the substrate x_d is of the order of 100 μm to 1 mm and it grows as a function of time, we consider that the dominant factor for the deformation is the effect of the swelling (Another possible factor which causes the deformation of the substrate is the balance between the capillary force and elastic force.[12,14] However, the characteristic size of x_d in that case is considerably smaller: $x_d \approx \gamma/E$ is of the order of 1 μm for E = 25 kPa[14,24]).

Here we consider the diffusion of water into the gel with an analogy of the drying problems of the droplet.[30,31] Due to the geometry of the droplet, it is expected that the diffusive flux of water near the edge of the droplet is strongly enhanced compared to the center (Fig. 10(a)). Therefore, the substrate in the vicinity of the contact line swells with water quite rapidly, and it forms a "locally swollen" region. Once it is formed, the contact line feels the surface of this locally swollen region, and whether the contact line can recede or not is determined by the wetting property of the swollen gel surface. (Fig. 10(b)).

To check the wetting property of the swollen gel surface, we conducted a supplemental wetting experiment on a gel substrate which is previously fully swollen in a water bath. To avoid that a thin water layer could remain on the gel surface, the level of the

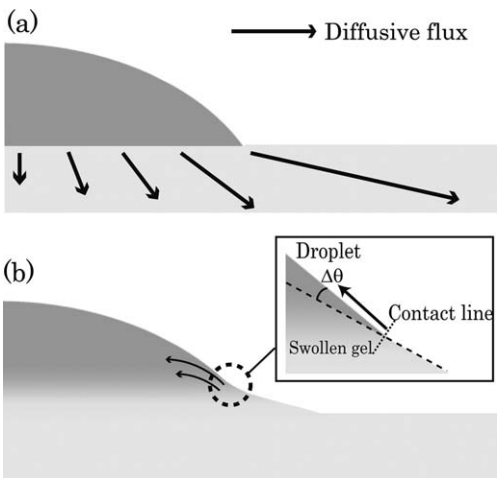

Fig. 10 The mechanism of the recession of the contact line. (a) The initial stage that the contact line is pinned. For geometrical reasons, diffusive flux from the droplet to the gel is strongly enhanced near the contact line. (b) The second stage where the contact line recedes. Due to the water diffusion, a locally swollen region has formed near the contact line. For the contact line to recede, the actual contact angle $\Delta\theta$ (the angle with respect to the slope of the substrate) must correspond to the equilibrium contact angle on this swollen gel surface.

water bath is always kept below the gel surface during the swelling process, and the gel surface was softly wiped with an optical cleaning tissue (Kimwipes; Kimberly-Clark Professional, USA) before being used. We observed that on a fully swollen gel substrate, the droplet spreads rapidly and the contact angle takes a considerably small value (<3°) irrespective of the MBA concentration and AMPS concentration. (This result can be understood in terms of the thermodynamic equilibrium. Since the fully swollen gel is equilibrated with the bulk water, putting a water droplet on the fully swollen gel is thermodynamically nearly the same condition as putting a water droplet on a bulk water, where the droplet spreads completely.)

From the results of the supplemental experiment, it is expected that the equilibrium contact angle on the locally swollen gel surface is very close to 0°. For the contact to recede on a gel substrate, the actual contact angle of the droplet with respect to the slope of the substrate $\Delta\theta = \theta_{\mathrm{drop}} - \theta_{\mathrm{gel}}$ must correspond to the equilibrium contact angle on a swollen gel surface. Therefore, the contact line is pinned until $\Delta\theta$ reaches nearly 0°.

The negative dependence of $t_{\mathrm{rec}}/t_{\mathrm{f}}$ on the volume swelling ratio of the substrate $V_{\mathrm{gel}}^{\mathrm{sw}}/V_{\mathrm{gel}}^{\mathrm{i}}$ in Fig. 9(c) can be understood in terms of the growth of the deformation of the gel surface. For the gel substrate with a large swelling ratio, after a droplet is placed on the substrate, the region near the water–gel interface changes its volume drastically by swelling with water, which causes the large rise of the gel surface around the droplet. Therefore, the angle of the local slope of the gel surface at the contact line θ_{gel} increases rapidly up to the value of θ_{drop} at an early stage of the diffusion process. On the other hand, for the substrate with a small swelling ratio, the rise of the gel surface due to the swelling effect is relatively small. In that case, θ_{drop} does not correspond to θ_{gel} until the droplet diffuses most of water into the gel and decreases θ_{drop} to considerably a small value.

B. Analysis for characteristic time of contact line recession

In this section, we propose a modeling for estimating the time of the contact line recession. Here we consider a simple model depicted in Fig. 11 to get the order of magnitude for the behaviors of θ_{drop} and θ_{gel} at the initial pinned-contact line stage.

We assume that below the droplet, the water diffusion creates the diffusive boundary layer of typical thickness $\sqrt{Dt}$, where D is the diffusion coefficient of water in the gel. The typical volume flux of water at the water–gel interface $z = z_{\mathrm{gel}}$ is scaled as

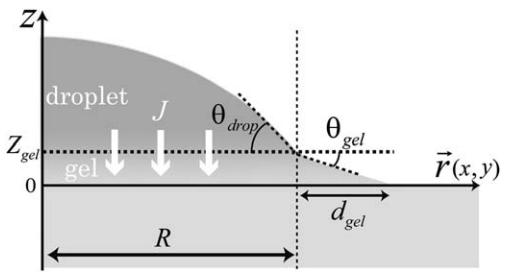

Fig. 11 Geometry, coordinates, and variables of the system in the theoretical modeling.

$$J \sim D\frac{\phi_{\mathrm{sw}} - \phi_{\mathrm{i}}}{\sqrt{Dt}}. \tag{7}$$

where ϕ_{sw} is the volume fraction of water in the fully swollen gel (suppose that at the water–gel interface, gel is immediately swollen), and ϕ_{i} is the volume fraction of water in the gel at the initial state. Due to this flux, the volume of the droplet $\mathrm{d}V_{\mathrm{drop}} \approx \pi R^3\theta_{\mathrm{drop}}$ decreases as

$$\frac{\mathrm{d}V_{\mathrm{drop}}}{\mathrm{d}t} \approx \pi R^3\frac{\mathrm{d}\theta_{\mathrm{drop}}}{\mathrm{d}t} = -\pi R^2 J. \tag{8}$$

while the volume of the gel increases as

$$\frac{\mathrm{d}V_{\mathrm{gel}}}{\mathrm{d}t} \approx \pi R^2\frac{\mathrm{d}z_{\mathrm{gel}}}{\mathrm{d}t} = \pi R^2 J. \tag{9}$$

The local slope of the gel near the contact line θ_{gel} is estimated to be close to the ratio $z_{\mathrm{gel}}/d_{\mathrm{gel}}$, where z_{gel} designates the vertical displacement of the droplet basis due to swelling, and d_{gel}, the horizontal distance on which this displacement relaxes radially around the droplet. With an analogy of a contact problem of solid bodies,[32] here we assume that the shape of the gel surface is mainly dictated by a compromise between the shear elasticity of the gel and the rising condition $z = z_{\mathrm{gel}}$ at the droplet basis of radius R. The characteristic size of d_{gel} is thus estimated as the same order of the droplet radius: $d_{\mathrm{gel}} \sim R$. (Rigorously, the water diffusion in a horizontal direction affects the shape of the gel surface in addition to the deformation due to the rise of the droplet basis. However, at an early stage where the characteristic size of the swollen region in a horizontal direction $x_{\mathrm{gel}} \approx z_{\mathrm{gel}} \sim (\phi_{\mathrm{sw}} - \phi_{\mathrm{i}})\sqrt{Dt}$ is sufficiently smaller than the size of the droplet R, this effect can be neglected.)

Combining eqns (7)–(9), the time evolution of the angles θ_{drop} and θ_{gel} are obtained as

$$\theta_{\mathrm{drop}}(t) - \theta_{\mathrm{drop}}^{(0)} \sim -\frac{\phi_{\mathrm{sw}} - \phi_{\mathrm{i}}}{R}\sqrt{Dt}. \tag{10}$$

$$\theta_{\mathrm{gel}}(t) \sim \frac{\phi_{\mathrm{sw}} - \phi_{\mathrm{i}}}{R}\sqrt{Dt}. \tag{11}$$

where $\theta_{\mathrm{drop}}^{(0)}$ is the initial value of the effective contact angle of the droplet. Eqns (10) and (11) predict that the time evolutions of $\theta_{\mathrm{drop}}(t) - \theta_{\mathrm{drop}}^{(0)}$ and of $\theta_{\mathrm{gel}}(t)$ are proportional to $\sqrt{t}$. In Fig. 8, the fitting curves ($a + b\sqrt{t}$ with fitting parameters a and b) are drawn for θ_{drop} and θ_{gel} as dashed lines. Except for the data of θ_{gel} at a very early stage in Fig. 8(a) (where the experimental uncertainty is not negligible), the experimental data fits the curves well.

From eqns (10) and (11), the characteristic time of the contact line recession τ, *i.e.*, the time when the actual contact angle $\Delta\theta = \theta_{\mathrm{drop}} - \theta_{\mathrm{gel}}$ goes to zero, is thus estimated as

$$\tau \sim \frac{\left(R\theta_{\mathrm{drop}}^{(0)}\right)^2}{D(\phi_{\mathrm{sw}} - \phi_{\mathrm{i}})^2}. \tag{12}$$

Let us calculate τ for our gel ($C_{\mathrm{MBA}} = 5$ mol%, $C_{\mathrm{AMPS}} = 10$ mol %): $R = 1.42$ mm, $\theta_{\mathrm{drop}}^{(0)} = 27.1°$, and $\phi_{\mathrm{sw}} - \phi_{\mathrm{i}} = 0.0529$ (obtained by the data of swelling ratio). For the diffusion coefficient D, we refer to the data in ref. 33: the value which is closest to our system is AAm/AMPS in water (AMPS/mg = 300) in Table 5: $D = 39.47 \times 10^{-8}$ m^2 s^{-1}. By substituting these values in eqn (12), τ is

calculated as *ca.* 400 s. Experimentally, the time for the onset of the contact line recession was measured as 140 s, which is not far from our theoretical estimation.

V. Conclusion

In this article, we have studied the dynamics of the wetting and diffusing processes of water droplets on hydrogel (Poly (2-acrylamido-2-methyl-propane-sulfonic acid -*co*- acrylamide) (PAMPS–PAAM)) substrates. The profiles of the droplet and substrate were measured dynamically using a grid projection method. We have observed that as the water droplet diffuses into the gel, the behavior of the contact line successively exhibits two different regimes: pinned and receding, and the transition between these two regimes is closely related to the local deformation of the gel substrate. The contact line is initially pinned after the droplet is placed. As the water diffusion proceeds, the effective contact angle of the droplet decreases while the angle of the local slope of the gel surface near the contact line increases. Finally these two angles almost correspond to each other, and it is at this moment that the contact line starts to recede. This result indicates that at the moment of the contact line recession, the actual contact angle is nearly 0°. We have also discussed how the pinned–receding transition depends on the properties of the gel substrate such as the rigidity and hydrophilicity, and have found that the length of the initial pinned regime largely depends on the gel swelling ability.

About the mechanism of the pinning–receding transitions of the contact line, we have proposed a physical model that a locally swollen region is formed in the vicinity of the contact line, and that whether the contact line is pinned or recedes is determined by the wetting property of this swollen region. This model correctly reproduces the evolutions of the droplet and gel angles at the initial pinned-contact line stage, and explains the effect of the gel swelling ability on the length of the initial pinned regime.

Our results show that the dynamics of the contact line on hydrogel substrates are quite different from those observed for general solid materials, especially for the coupling between the pinning–receding transition of the contact line and the angles of the droplet and substrate. Further studies are required for the detailed analysis of the present phenomena, especially for the late stage of the diffusion process where the contact line recedes and the swollen region grows up to the size of the droplet. This would be possible by solving the combined equations of the water transport from the droplet to gel and of the balance of interfacial tensions at the contact line, which will be expected in future works.

Acknowledgements

The authors gratefully thank Y. Shimokawa, K. Sakai and M. Doi (Tokyo University) for discussions about the theoretical and experimental parts of this work.

References

1 M. Doi, *J. Phys. Soc. Jpn.*, 2009, **78**, 052001:1–19.
2 N. A. Peppas, P. Bures, W. Leobandung and H. Ichikawa, *Eur. J. Pharm. Biopharm.*, 2000, **50**, 27–46.
3 J. Yang, M. Yamato, C. Kohno, A. Nishimoto, H. Sekine, F. Fukai and T. Okano, *Biomaterials*, 2005, **26**, 6415–6422.
4 J. P. Gong, T. Kurokawa, T. Narita, G. Kagata, Y. Osada, G. Nishimura and M. Kinjo, *J. Am. Chem. Soc.*, 2001, **123**, 5582–5583.
5 G. Kagata, J. P. Gong and Y. Osada, *J. Phys. Chem. B*, 2002, **106**, 4596–4601.
6 H. Kikuchi, K. Sakai and K. Takagi, *Jpn. J. Appl. Phys.*, 1991, **30**, L:1668–1670.
7 G. Wang, D. Chen, L. Lu, X. Wang and Y. Yang, *J. Coat. Technol.*, 1998, **70**, 55–59.
8 D. Julkowska, M. Obuchowski, I. B. Holland and S. J. Séror, *Microbiology*, 2004, **150**, 1839–1849.
9 P. G. de Gennes, F. B. Wyart and D. Quere, *Capillarity and Wetting Phenomena*, Springer, 2003.
10 P. G. de Gennes, *Rev. Mod. Phys.*, 1985, **57**, 827–863.
11 D. Bonn, J. Eggers, J. Indekeu, J. Meunier and E. Rolley, *Rev. Mod. Phys.*, 2009, **81**, 739–805.
12 M. E. R. Shanahan and P. G. de Gennes, *C.R. Acad. Sci. Paris*, 1986, **302**(Ser. II), 517.
13 M. E. R. Shanahan, *J. Phys. D: Appl. Phys.*, 1987, **20**, 945–950.
14 C. W. Extrand and Y. Kumagai, *J. Colloid Interface Sci.*, 1996, **184**, 191–200.
15 A. Carré and M. E. R. Shanahan, *Langmuir*, 1995, **11**, 24–26.
16 A. Carré, J. C. Gastel and M. E. R. Shanahan, *Nature*, 1996, **379**, 432–434.
17 A. Carré and M. E. R. Shanahan, *Langmuir*, 2001, **17**, 2982–2985.
18 L. Bacri and F. B. Wyart, *Eur. Phys. J. E: Soft Matter Biol. Phys.*, 2000, **3**, 87–97.
19 A. Tay, C. Monteux, D. Bendejacq and F. Lequeux, *Eur. Phys. J. E*, 2010, **33**, 203–210.
20 D. Szabó, S. Akiyoshi, T. Matsunaga, J. P. Gong and Y. Osada, *J. Chem. Phys.*, 2000, **113**, 8253–8259.
21 D. Kaneko, J. P. Gong, M. Zrínyi and Y. Osada, *J. Polym. Sci., Part B: Polym. Phys.*, 2005, **43**, 562–572.
22 Y. Nonomura, Y. Morita, T. Hikima, E. Seto, S. Chida and H. Mayama, *Langmuir*, 2010, **26**, 16150–16154.
23 R. P. Cámara, A. Best, H. J. Butt and E. Bonaccurso, *Langmuir*, 2008, **24**, 10565–10568.
24 R. P. Cámara, G. K. Auernhammer, K. Koynov, S. Lorenzoni, R. Raiteri and E. Bonaccurso, *Soft Matter*, 2009, **5**, 3611–3617.
25 E. R. Jerison, Y. Xu, L. A. Wilen and E. R. Dufresne, *Phys. Rev. Lett.*, 2011, **106**, 186103:1–4.
26 J. Kurata, K. T. V. Grattan, H. Uchiyama and T. Tanaka, *Rev. Sci. Instrum.*, 1990, **61**, 736–739.
27 M. Fermigier, L. Limat, J. E. Wesfreid, P. Boudinet and C. Quilliet, *J. Fluid Mech.*, 1992, **236**, 349–383.
28 C. Andrieu, D. Chatenay and C. Sykes, *C.R. Acad. Sci. Paris*, 1995, **320**, 351–357.
29 M. Banaha, A. Daerr and L. Limat, *Eur. Phys. J. Spec. Top.*, 2009, **166**, 185–188.
30 R. D. Deegan, O. Bakajin, T. F. Dupont, G. Huber, S. R. Nagel and T. A. Witten, *Phys. Rev. E: Stat. Phys., Plasmas, Fluids, Relat. Interdiscip. Top.*, 2000, **62**, 756–765.
31 H. Hu and R. G. Larson, *J. Phys. Chem. B*, 2002, **106**, 1334–1344.
32 L. D. Landau and E. M. Lifshitz, *Theory of Elasticity*, Butterworth Heinemann, 3rd edn, 1986.
33 S. Kundakci, Ö. B. Üzüm and E. Karadağ, *React. Funct. Polym.*, 2008, **68**, 458–473.

